Journal of Materials Chemistry C

PAPER

Detonation nanodiamonds tailor the structural order of PEDOT chains in conductive coating layers of hybrid nanoparticles

Cite this: *J. Mater. Chem. C*, 2014, **2**, 3703

Emanuela Tamburri,*[a] Valeria Guglielmotti,[b] Roberto Matassa,[c] Silvia Orlanducci,[a] Stefano Gay,[a] Giacomo Reina,[ab] Maria Letizia Terranova,[a] Daniele Passeri[c] and Marco Rossi[c]

Received 30th November 2013
Accepted 13th February 2014

DOI: 10.1039/c3tc32375g

www.rsc.org/MaterialsC

Solid layers of PEDOT–detonation nanodiamond based nanoparticles with an exceptional structural order were produced by means of a template-free polymerization technique. As an efficient multifunctional filler, the nanocrystalline diamond has been shown to possess a high catalytic activity on the monomer polymerization rate as well as to play a fundamental role as a 3D arrangement-directing agent of the PEDOT chains at the micro- and nano-scale. SEM, TEM and TED analyses highlighted the mutual organization between PEDOT oligomers and nanodiamond grains, and the produced hierarchical effects on the arrangement of the backbones of the final polymer. Optical and Raman spectroscopy, used together with XRD diffraction to study the molecular structure and crystallographic features of the hybrid materials, pointed out that the adopted synthetic strategy enables highly conjugated and doped hybrid systems to be generated. The spatial distribution of the filler inside the polymeric matrix and the mutual connectivity of nanodiamond crystals and PEDOT segments are found to strongly improve the functional properties of the host polymer. Mechanical characterizations by advanced AFM-based techniques revealed that both indentation modulus and hardness of PEDOT/nanodiamond materials are 3 times higher than the pure PEDOT polymer, while electrical characterizations by a 4-probe method gave sheet resistance values of 1×10^6 Ω sq^{-1} for the nanocomposite particles.

1. Introduction

Conducting polymers (CP) are the fourth generation polymeric materials. Their electrical conductivity can be increased by many orders of magnitude from 10^{-10}–10^{-5} to 10^{2}–10^{5} S cm^{-1} upon doping, thus covering in principle the whole insulator–semiconductor–metal range. Due to their special conduction mechanism, unique electrical properties, their reversible doping/dedoping process and their controllable chemical and electrochemical properties, CP show promising features for application in the next generation organic devices: chemical- and bio-sensors, field-effect transistors, photovoltaic cells, organic light-emitting diodes, field emission and electrochromic display devices, supercapacitors, *etc.* However, even if the electronic and electrochemical behavior of these materials is now relatively well understood, the next frontier to surpass is to develop the ability to control their morphology and crystallinity. In fact, although numerous publications have demonstrated that for many applications CP micro- and nanostructures exhibit clear advantages over their bulk counterparts, it is their morphology and 3D arrangement that ultimately affects the efficiency, longevity, and response time of the produced devices.[1]

A wide variety of lithographic, physical, and chemical approaches have been adopted for the preparation of micro- and nano-structured CP.[2] The chemical methodologies typically include the use of template-guided synthesis with (1) hard physical templates like anodized alumina membranes, porous membranes, mesoporous silica and zeolites, or (2) soft chemical templates like interfacial polymerization, template-free method, dilute polymerization, reverse emulsion polymerization, *etc.* The use of such structure-directing templates enables access to a large variety of micro/nanostructure morphologies including tubes, fibers, microspheres, nanoparticles, nanowires and mesocellular foams.[2] Although hard-template-assisted polymerizations can produce conducting polymers with well-defined nanoscale features, it is not always possible to have a control on the spatial organization of the polymer chains, and moreover this method can be unsatisfactory for fabricating cost-effective

[a]*Dip.to di Scienze & Tecnologie Chimiche - MinimaLab, Università di Roma "Tor Vergata", Via Della Ricerca Scientifica, 00133 Rome, Italy. E-mail: Emanuela.Tamburri@uniroma2.it*

[b]*NanoShare srl, Via G. Peroni 386, 00131 Rome, Italy*

[c]*Dip.to di Scienze di Base e Applicate per l'Ingegneria & Centro di Ricerca per le Nanotecnologie applicate all'Ingegneria (CNIS), Università degli Studi di Roma "Sapienza", Via A. Scarpa, 00161 Rome, Italy*

nanostructures in large volumes. In this view, the use of synthetic approaches adopting template-free methods can be considered much more advantageous.[3,4]

In this context, searching for alternative synthesis routes we investigated the effects of ultrananocrystalline diamond (ND) particles on the template-free growth of nanoscale polyaniline structures during both electrochemical and chemical polymerization.[5–7] The nanodiamond produced by detonation of carbon-containing explosives represents a special class of diamond materials with the characteristic size encompassing the range of just a few nanometers.[8] This new member of the carbon family has opened a new era in materials science, and the related technology is growing at a very high speed, due to the fact that ND possesses a number of attractive properties, conferred by the unusual values of surface energy and by confinement effects.[9]

In our research directed to the study of the aniline polymerization in the presence of ND, we evidenced the occurrence, between diamond particles and aniline oligomeric segments, of mutual interactions able to modulate the structure and final morphology of the polyaniline–nanodiamond systems. Such stimulating findings have led us to expand our studies on one of the most successfully conducting polymers, poly(3,4-ethylenedioxythiophene) (PEDOT). This polymer is characterized by a remarkably high conductivity and an excellent environmental stability, which made PEDOT and its derivatives excellent candidates for several industry applications. Nowadays, PEDOT based systems are indeed the only CP materials that are commercially utilized as antistatic coatings and electrode materials in organic semiconductor devices and electrical connections. Therefore, on the basis of the undeniable interest that these materials arouse, not only in the academic community, but also in the industry field and after having intensely examined synthesis conditions, electroactive and electrical behavior of electropolymerized PEDOT films,[10–12] in the present research we have focused our efforts on the preparation by template-free methods of PEDOT based composite nanoparticles using ND as a multifunctional filler.

Whereas a large variety of self-assembled polyaniline micro/nanostructures and composites has been obtained by template-free techniques,[2,13] only a few attempts have been made to use such approach for the synthesis of PEDOT micro- and nanomaterials,[14–19] and regarding the presence of ND, only one study about EDOT electropolymerization has been reported so far at the best of our knowledge.[20] In view of that, we found it noteworthy to investigate the effects of detonation nanodiamonds toward the template-free chemical polymerization of EDOT monomers in aqueous medium, and to detect a possible influence of diamond crystals on the 3D organization of PEDOT chains in the final material. In particular, a deep investigation of the structure and morphology of the hybrid nanoparticles produced under different experimental conditions, as well as of the electrical and mechanical properties of compact coating layers produced with the nanocomposite particles, has been carried out in order to have a comprehensive knowledge of these novel hybrid materials.

2. Experimental section

2.1 Reagents and methods

EDOT monomer was obtained from Aldrich and used as received. Ultrananocrystalline diamond particles produced by detonation were provided by the International Technology Center (USA). The anionic surfactant sodium dodecyl sulfate (SDS) purchased from Aldrich was used as a stabilizer of the reaction environment as well as a charge-balancing dopant during polymerization. Chemical polymerizations were carried out in distilled water by using ammonium peroxydisulfate (APS) (Aldrich) as an oxidant. Different molar ratios among EDOT, APS and ND were investigated. All the mixtures were reacted for 5 days under stirring at 0–5 °C in an ice bath. After that, a dialysis cleaning of the polymer dispersions was carried out under constant stirring for one week at room temperature in order to reduce the concentration of unreacted reagents.

2.2 Characterization techniques

The size of the ND particle dispersions was determined by dynamic light scattering (DLS) using a Malvern NanoZetaSizer spectrometer, equipped with a 5 mW HeNe laser ($\lambda = 632.8$ nm) and a digital logarithmic correlator. The measurements were carried out at a scattering angle of 90°. The electrophoretic mobility of ND particles was measured by means of the laser Doppler electrophoresis technique using the Malvern NanoZetaSizer apparatus. The mobility μ was converted into the ζ-potential using the Smoluchowski relation $\zeta = \mu\eta/\varepsilon$, where η and ε are the viscosity and the permittivity of the solvent phase, respectively.

PEDOT and PEDOT–ND samples were investigated by means of different characterization techniques. The chemical structure was analyzed by optical and Raman spectroscopy. Optical spectra were recorded with a UV-1800 Shimadzu spectrophotometer. Raman studies were performed by using a XploRA ONE™ Raman Microscope (Horiba Jobin Yvon) using a 532 nm excitation laser light and a 2400 gr mm^{-1} grating spectrometer coupled with an air-cooled scientific CCD. The study of the crystalline structure was performed by X-ray diffraction (XRD) and a Seifert-XRD3003 diffractometer with a Bragg–Brentano geometry, employing a Cu Kα source ($\alpha = 1.54056$ Å), was used for the measurements. The morphology was studied by using a scanning electron microscopy FIB-SEM Cross Beam Workstation ZEISS Auriga, a helium ion microscopy Carl Zeiss Orion HIM at an accelerating voltage of 30 kV and at a beam current of 0.6 pA and a transmission electron microscopy FEI-TITAN TEM operating @80 and @300 kV. Electrical measurements were performed by a four-probes setup. The probes were connected to a Keithley 6221 current source and a Keithley 2700 multimeter. The system was connected to a PC by a Labview interface. Mechanical properties have been evaluated through atomic force microscopy (AFM) based nanoindentation. Cantilever deflections *versus* tip–sample distances have been acquired using a standard AFM apparatus (Icon, Bruker Inc.) equipped with a standard Si cantilever (NSC16, Mikromash, Estonia) with spring constant $k_c = 54$ N m^{-1}. The shape of the AFM tip has

been reconstructed analyzing the images obtained on a calibration grating constituted by an array of inverted tips (TGT1, NT-MDT, Russia). To evaluate the indentation modulus and hardness of the samples, the curves of cantilever deflection *versus* tip–sample distance have been analyzed using a procedure already reported.[21]

3. Results and discussion

3.1 Nanodiamond processing

Detonation nanodiamonds are typically constituted by primary particles with a size of ~4–5 nm formed by a diamond core and a graphene shell. A wide variety of functional groups can be found at the surface of such particles as a consequence of purification treatments. Thus, surface charges ranging from highly positive to highly negative can be typically found on the ND surface. Moreover, ND is rarely identifiable as a single crystal particle in solution, rather it is known to form tightly and loosely bound aggregates when dispersed in a solvent.[22] The nanodiamond particles used for the present study are found to form stable aqueous dispersions without the use of any particular surfactant and/or additive. Therefore ζ-potential and DLS analyses were performed on such dispersions in order to identify the charges that may be present on the surface of ND particles as well as the size of the stable aggregates formed in solution. The measurements revealed that the ND particles are dispersed in water as aggregates with an average diameter of about 95 nm and a large positive electrophoretic mobility of 2.8×10^{-8} $m^2 V^{-1} s^{-1}$, which corresponds to a ζ-potential of about +36 mV. The origin of a positive ζ-potential for ND is still debated, however protonated forms of pyrone-like structures seem to be the surface groups mainly responsible for a positive zeta-potential of ND possessing residual aromatic rings at the surface.[22] Regardless of the chemical nature of the functional groups, the high value found for the potential undoubtedly indicates that the ND is well dispersed in water and that the produced ND dispersions can be exploited as a suitable reaction environment for the subsequent PEDOT growth.

3.2 Polymers and nanocomposites synthesis

EDOT is a chemical compound insoluble in water, and an oil-in-water emulsion is typically formed when it is mechanically forced to disperse into an aqueous medium. Therefore SDS was added to the reaction mixture in order to increase the emulsion stability and, consequently, the yield of EDOT polymerization. In this way a twofold advantage was obtained in one step. In fact, if from one side the surfactant stabilizes the EDOT–water system, from another one a surfactant containing anionic functional groups, like SDS, can behave as an efficient dopant for the PEDOT matrix. Therefore, we performed a series of polymerization reactions by keeping the molar concentration of SDS constant and by properly varying the molar ratio among EDOT, APS, and ND as reported in Table 1. Peroxodisulfates are the best peroxidic oxidants for EDOT to form conductive PEDOT systems and the overall chemical reaction between EDOT and APS can be written as reported in Fig. 1 with dodecyl sulfate as the dopant counterion. For each experiment, before addition of APS, the EDOT-SDS and EDOT-SDS-ND aqueous dispersions were subjected to power ultrasounds to produce stable colloidal emulsions. In fact, the monomer droplets formed by the strong mechanical treatment are expected to be stabilized by the surfactant molecules, which arrange themselves with their hydrophobic tails on the outer surface of the droplets. This architecture represents the starting seed for the subsequent polymerization process and should act as a sort of soft-template for the production of PEDOT nanostructures.

Table 1 Molar ratios among the reagents EDOT, APS and ND and starting times for polymerization reactions for the pure polymer (EA, $EA_{1/2}$, $EA_{1/4}$) and composite (EAD, $EA_{1/2}D$, $EA_{1/4}D$) samples

Sample	EDOT	APS	ND	Reaction starting time
EA	1	1	0	4 h
EAD	1	1	1	45′
$EA_{1/2}$	1	1/2	0	7 h
$EA_{1/2}D$	1	1/2	1	2 h
$EA_{1/4}$	1	1/4	0	>10 h
$EA_{1/4}D$	1	1/4	1	4 h 20′

The first observation concerning the course of the reaction was the remarkable reduction of the activation time of the polymerization process in the presence of nanodiamonds (Table 1). We arbitrarily referred this time to the appearance of a light blue coloration of the solution that is compatible with the formation of the PEDOT chains. The PEDOT chemical growth mechanism is an addition polymerization, where a coupling between a radical and a monomer typically occurs in the bulk of the reaction environment.[23] Therefore the chain initiation requires the generation of highly reactive radical EDOT ions. According to this reaction pathway and to the stoichiometry of the polymerization reaction from EDOT to PEDOT (Fig. 1), we observed an increase of the activation time from 4 h to >10 h on lowering the concentration of the APS radical initiator (see data for EA, $EA_{1/2}$ and $EA_{1/4}$ samples in Table 1). Conversely, for

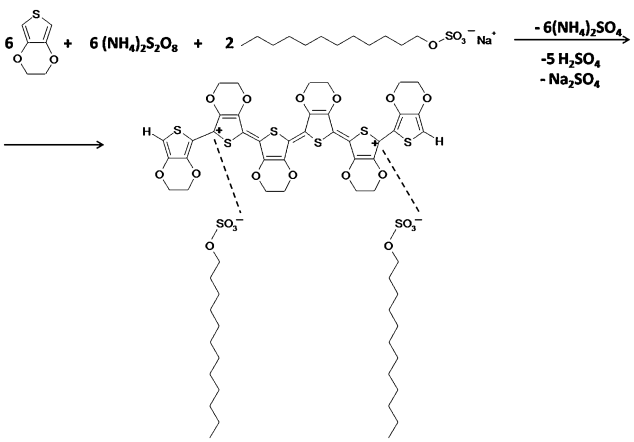

Fig. 1 Reaction of EDOT oxidative polymerization to PEDOT–dodecyl sulfate initiated by APS. The reaction is depicted for the hexamer formation for simplification.

reactions carried out under the same conditions but in the presence of ND, the polymerization took place with activation times from a minimum of 45 minutes to a maximum of 4 h 30′ (see data for EAD, $EA_{1/2}D$ and $EA_{1/4}D$ samples in Table 1). Such a result seems to indicate that ND dispersed in the bulk suspension plays a crucial role in the kinetics of the EDOT polymerization process and suggests a catalytic effect of such a filler on the radical reaction of the monomer. In order to deeply investigate the effects induced by ND, an attempt to polymerize EDOT in the presence of such a filler but without APS was also carried out. In this case no appreciable sign of polymerization was detected within 24 hours. The polymerization instead occurred when a very low amount (molar concentration of 1/5 with respect to the one of EDOT and ND) of a less strong oxidizing agent, like H_2O_2 in acidic aqueous solution,[24] was added. In the absence of ND, about 15 hours were required to start the reaction, whereas the time was reduced to about 10 h in the presence of ND. Taken as a whole, these studies point out that ND effectively participates in some way in the EDOT polymerization process.

Actually, as it has been emphasized in different studies, detonation nanodiamond itself, *i.e.* in the absence of a specific catalyst, has proved to possess catalytic activity towards some reactions.[25–28] Several explanations have been furnished for such capability and can be invoked to elucidate the action of ND in the polymerization reaction under consideration. First, the typical spheroid spatial arrangement of ND can provide an efficient access for the reactants, which can take advantage of the interactions with the surrounding graphene hexagonal cell as a π-conjugated system. Because of partial delocalization of the π-electron density, the curvature of the graphene layer could thus supply a superior activity in the electron transfers during the polymerization reaction.[26,29] In addition, a fundamental task can be undoubtedly played by the high surface reactivity owned by this intriguing material. In fact, the facet dependent variations of the surface electrostatic potential and the surface chemical functionalities can enable ND to be much more active and selective than other carbon materials.[27,30] This ability could be rationalized assuming the involvement of the positively charged functional groups evidenced on the ND surface by the ζ-potential measurements as well as of the radical species typically present on the ND surface.[31–33] In fact, these features could play a basic role in promoting the self-assembly onto the ND surface of the anionic surfactant micelles stabilizing the monomer droplets, and in the subsequent production of EDOT radical cations to form PEDOT nanoparticles *via* a soft-template synthesis route. The mechanism proposed is schematically depicted in Fig. 2. Moreover, the large surface-to-volume ratio of the ND aggregates endows numerous sites suitable for the occurrence of such phenomena.

Finally, causes more physical in nature can be also claimed as further contributions in supporting and speeding up the polymerization rates. In fact, the extremely high thermal conductance of the sp^3 diamond core of ND grains is expected to improve heat-transfer from the active sites, thus favoring dissipation of the heat produced by the exothermic radical polymerization process.

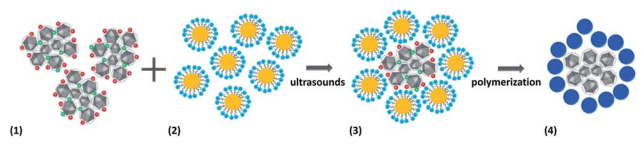

Fig. 2 Depiction of the mechanism proposed for the soft-template synthesis route followed by the reagents during the preparation of the hybrid PEDOT–ND nanoparticle systems: (1) stable ND aggregates functionalized by positively charged (red dots) and radical (green dots) species; (2) EDOT monomer droplets stabilized in water by means of the anionic surfactant micelles; (3) self-assembly onto the ND aggregates surface of the EDOT–dodecyl sulfate surfactant systems; and (4) PEDOT nanospheres (blue circles) grown and assembled on nanodiamond grains.

3.3 Structure and morphology

3.3.1 Molecular analysis. The molecular structures of PEDOT chains of the pure and nanocomposite samples have been investigated by optical and Raman spectroscopy. Fig. 3 depicts the absorption spectra of all the samples. Although the absorption spectrum of chemically polymerized PEDOT may result from various chemical species present, it is a common understanding that the main contribution stems from chains consisting of 5 up to 15 monomeric units. In the neutral totally reduced state, such chains typically produce a broad absorption peak covering the visible region, with a maximum in the 550–600 nm range, corresponding to the energy gap between π and π*. Broad absorption bands in the visible and in the IR region are instead generated from excitations of mid-gap states related to the free charge carriers (polarons or bipolaron states) associated with the oxidized forms of the chains. Therefore the feature of the absorption spectrum of PEDOT strongly depends on its backbone oxidation state.[34] In our case, we observe some differences between the spectra of the pure and composite materials. First of all, the presence of broad bands in the 300–600 nm range for all the spectra of the pure systems (EA, $EA_{1/2}$,

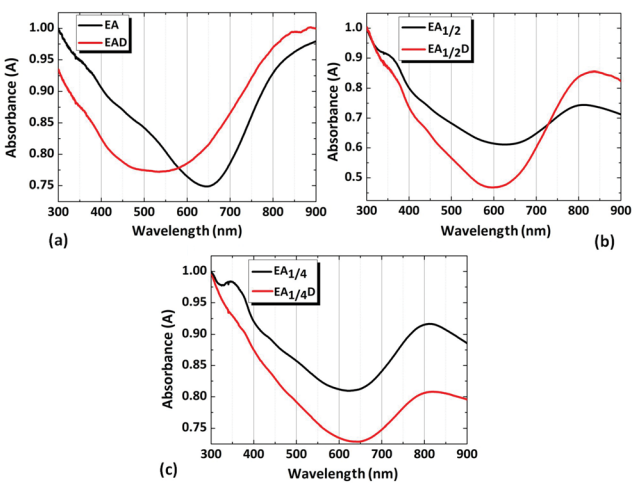

Fig. 3 Absorption spectra of pure PEDOT and PEDOT–ND composite samples: (a) EA and EAD; (b) $EA_{1/2}$ and $EA_{1/2}D$; (c) $EA_{1/4}$ and $EA_{1/4}D$.

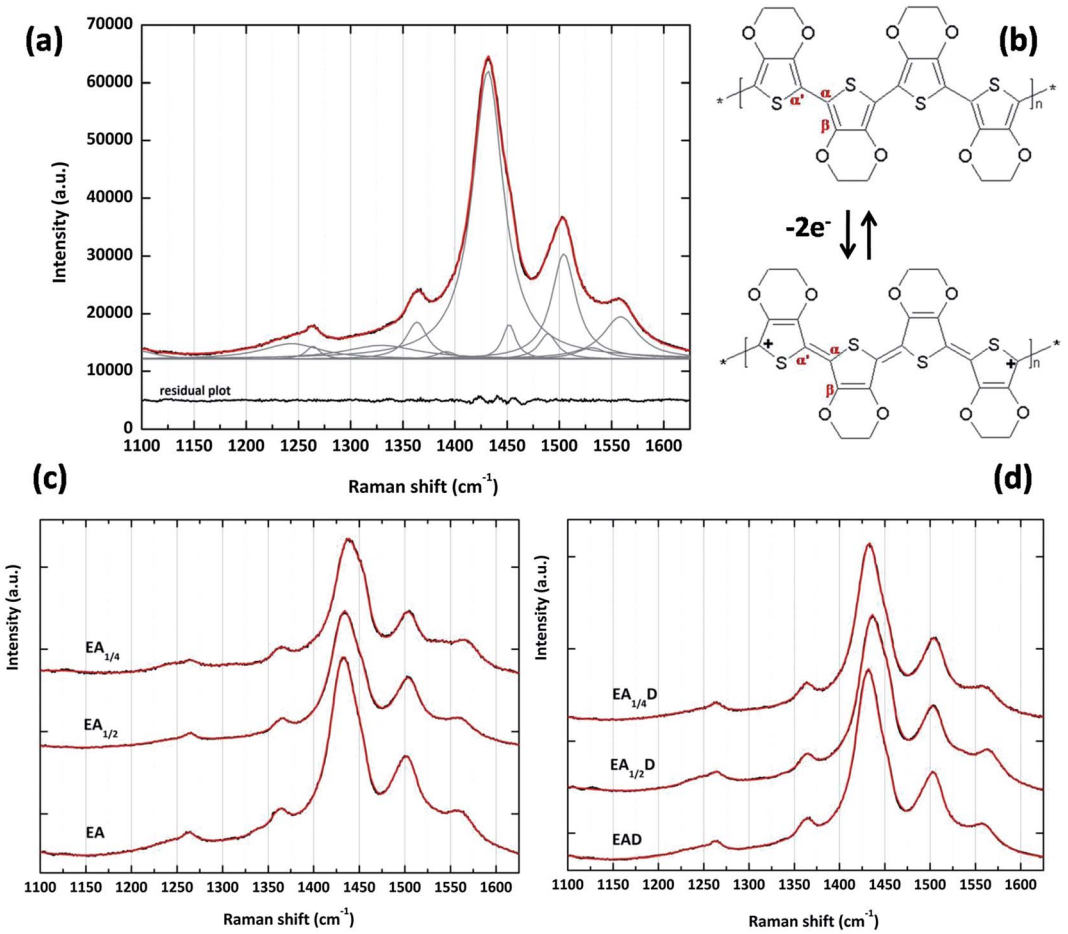

Fig. 4 Raman spectra of the samples in the frequency range 1100–1600 cm^{-1}: (a) Raman spectrum of the EAD sample with the bands resulting from the fitting; (b) sketch of the redox between the totally reduced and quinonoid totally oxidized form of the PEDOT backbone; (c) spectra of EA, $EA_{1/2}$ and $EA_{1/4}$ samples; (d) spectra of EAD, $EA_{1/2}D$ and $EA_{1/4}D$ samples.

$EA_{1/4}$) and of a more defined signal at ~350 nm for the $EA_{1/4}$ sample is noticeable. These bands can be interpreted as the contribution of oligomeric species constituted by 2,3 or 4 EDOT units, the dimers being mainly responsible for the absorption at 350 nm.[34] These signals are less evident in the PEDOT–ND composites meaning that when ND is present in the polymerization environment, the polymer chains are probably formed by a higher number of monomers. Moreover, the high transparency in the visible spectral range characterizing highly doped PEDOT systems can be noted in the EAD spectrum,

Table 2 Experimental Raman band wavenumbers (cm^{-1}) and vibrational assignments of PEDOT and ND[a]

Assignment	EA	EAD	$EA_{1/2}$	$EA_{1/2}D$	$EA_{1/4}$	$EA_{1/4}D$
$C_\alpha - C_{\alpha'}$ (inter-ring) str	—	1243 m	—	—	—	—
$C_\alpha - C_{\alpha'}$ (inter-ring) str	1262 vw	1264 w	1264 vw	1262 vw	1264 vw	1264 vw
ND	—	1329 m	—	1325 m	—	1327 vvw
$C_\beta - C_\beta$ str	1362 w	1363 m	1364 w	1364 w	1362 w	1363 w
$C_\beta - C_\beta$ str	—	1394 w	—	—	—	—
$C_\alpha{=}C_\beta$ sym str	1432 vs	1433 vs	1433 vs	1434 vs	1433 s	1432 vs
$C_\alpha{=}C_\beta$ sym str	1451 m	1452 m	1452 w	1453 w	1454 m	1452 w
$C_\alpha{=}C_\beta$ sym str or sp^2 from ND	1487 m	1491 w	—	1490 w	—	1489 w
$C_\alpha{=}C_\beta$ asym str	1502 s	1505 s	1503 s	1503 s	1501 s	1504 s
$C_\alpha{=}C_\beta$ asym str	1531 m	1533 m	1537 w	1536 vw	1535 w	1539 w
$C_\alpha{=}C_\beta$ asym str	1562 m	1560 m	1560 m	1563 m	1563 m	1561 m
$C{=}C$ str	1607 br	—	1613 br	1616 br	1618 br	1616 br
Conjugation length	2.8	4.25	2.0	2.6	1.9	2.5

[a] Key: str, stretching; asym, asymmetric; sym, symmetric; def, deformation; vs, very strong; s, strong; m, medium; w, weak; vw, very weak; br, broad.

where the onset of a band in the near-infrared range, at around 850 nm, is also distinguished (Fig. 3a). Such a signal, blue-shifted in the spectra of $EA_{1/2}$, $EA_{1/2}D$, $EA_{1/4}$ and $EA_{1/4}D$, can be ascribed to a transition involving one of the new electronic states generated inside the energy gap and related to oxidized PEDOT chains. These energy levels typically form bands with undefined features due to both the length distribution of PEDOT segments and the interaction of charge carriers. Moreover, at high doping levels these bands are characterized by a significant bathochromic shift of the absorption.[34]

Further information is derived by the analysis of the Raman spectra (Fig. 4). In general, a gradual broadening of the spectral lines is observable in the spectra collected from the samples synthesized by decreasing amounts of APS. Moreover, the pure polymer samples provide signals which are always broader than the ones related to nanocomposites. The Lorentzian fitting of the peaks found in the 1100–1650 cm^{-1} spectral range permits identification of several bands whose assignments, made on the basis of ref. 35–38, are summarized in Table 2. In Fig. 4a the Raman spectrum of the EAD sample with the bands resulting from the fitting is shown for more

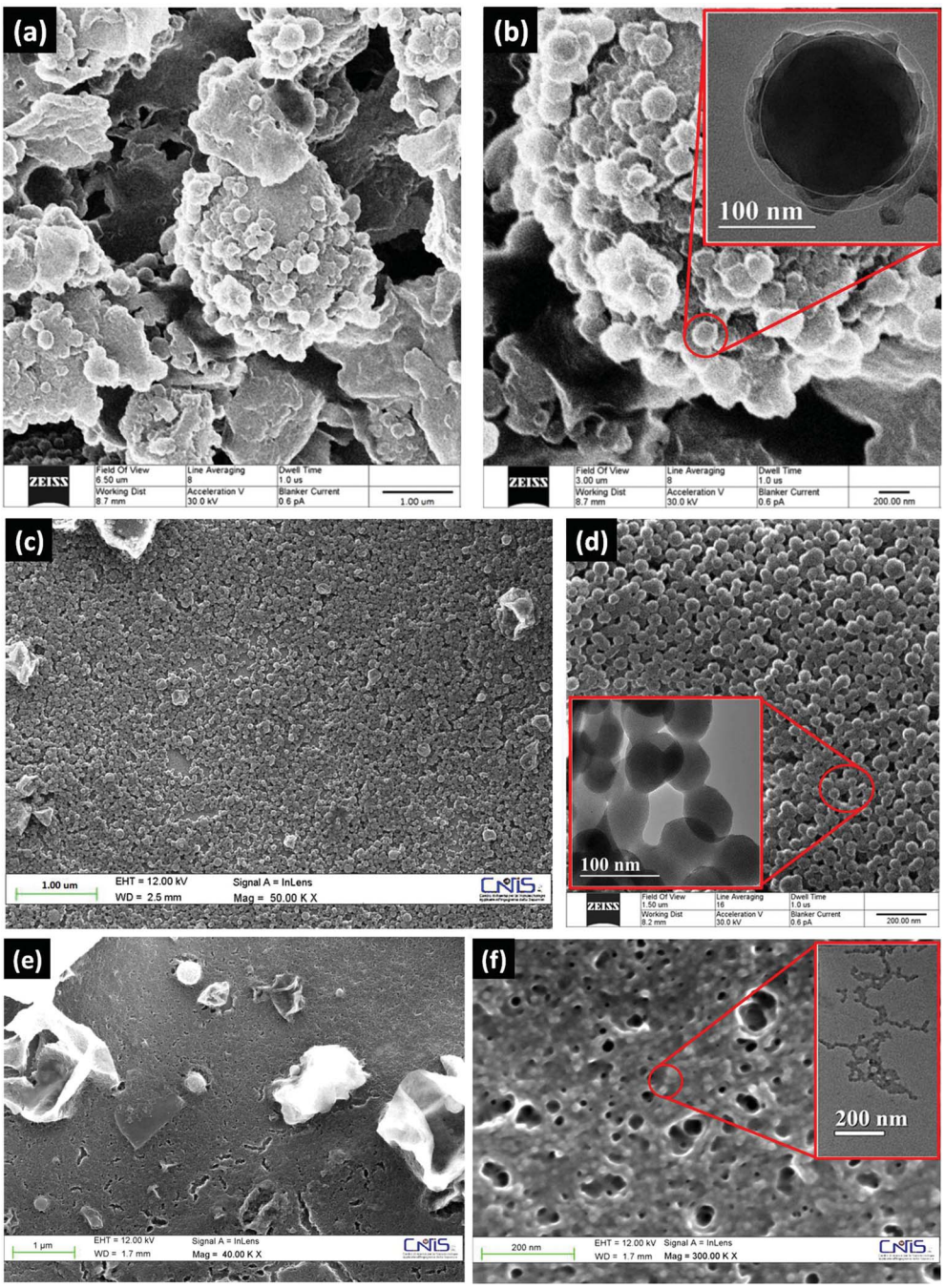

Fig. 5 Pictures at different magnifications of pure PEDOT samples: (a and b) HIM images of EA; (c) SEM and (d) HIM images of $EA_{1/2}$ and (e and f) SEM images of $EA_{1/4}$. Insets of Fig. 4b, d and f show TEM photos of the relating samples.

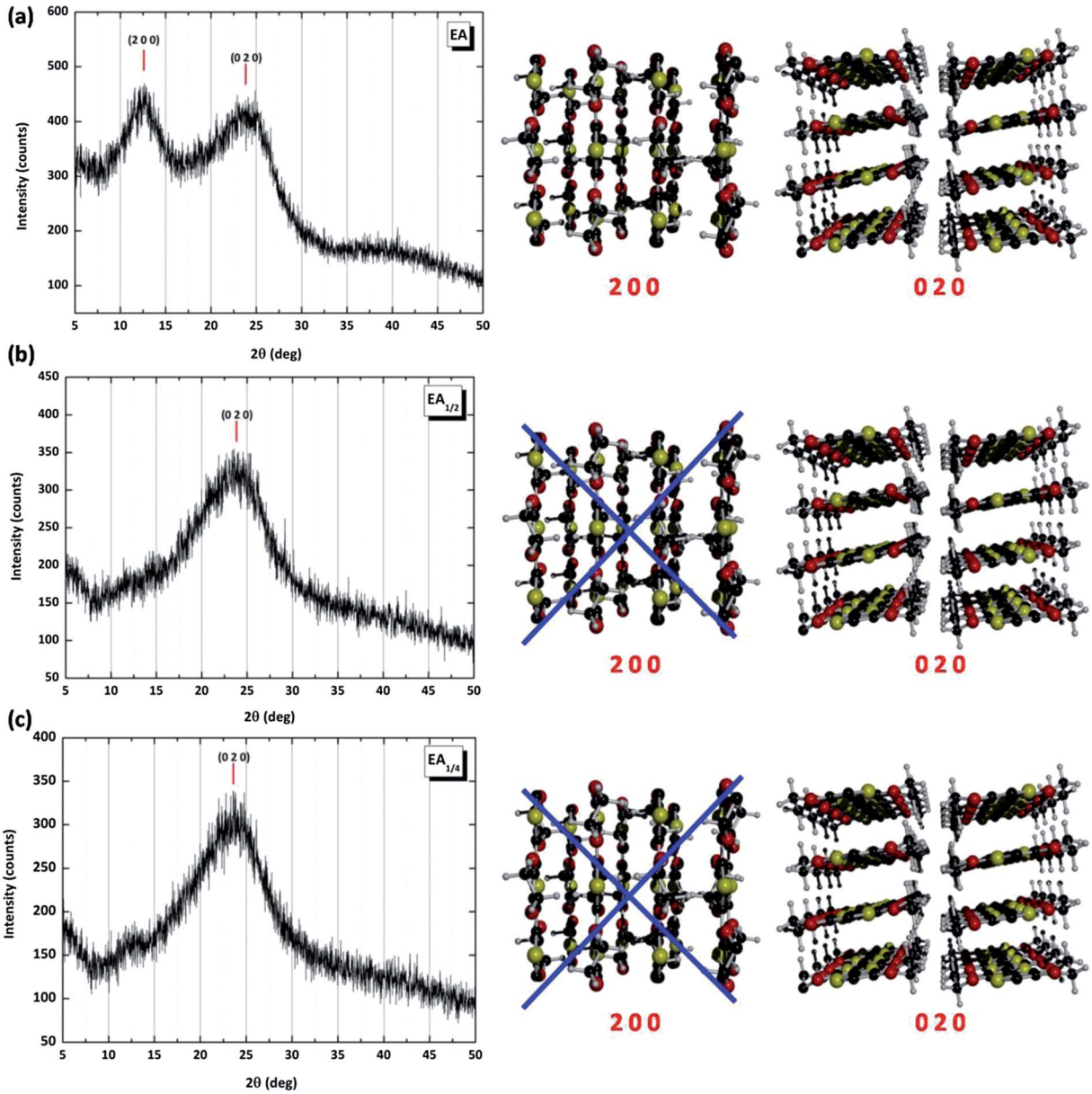

Fig. 6 XRD spectra and depictions of parallel (200) and normal (020) periodicity of the polymer backbones of pure PEDOT samples: (a) EA; (b) $EA_{1/2}$; and (c) $EA_{1/4}$.

clarity. For all samples, the Raman analysis indicates that the signals are essentially produced by oxidized chains for which a quinonoid form seems to prevail (see sketch in Fig. 4b). A frequency at about 1327 cm^{-1} ascribable to nanodiamond is also slightly visible in the composites spectra.[39] The major difference in the PEDOT molecular structure of the pure and composite samples concerns the conjugation length of the polymer chains, calculated as the intensity ratio $I(\upsilon_{C\alpha=C\beta sym})/I(\upsilon_{C\alpha=C\beta antisym})$.[40] It is possible to observe that all the polymers grown in the presence of ND possess a conjugation length (with values ranging from 2.5 to 4.25) that is longer than the one of the pure polymers (with values ranging from 1.9 to 2.8), and that the EAD sample has definitely the higher value (Table 2). Finally, some considerations can be done on the presence of the broad band at about 1607 cm^{-1}. It is not clearly observable in the EAD spectrum whilst it is found regularly blue shifting in the spectra of the other samples obtained by decreasing APS concentration. This band has been associated with short oligomers, or with defects in the π conjugation of the PEDOT backbone.[41] Such a result agrees with the absorption data and may explain the weak fluorescence detected in the spectra. Taking into account all the results of the molecular analysis, it is reasonable to conclude that ND, in general, promotes the formation of longer polymer chains, and for the same molar concentration of EDOT and APS in the SDS micellar solution (like the sample EAD), ND contributes to produce a highly conjugated and doped PEDOT system.

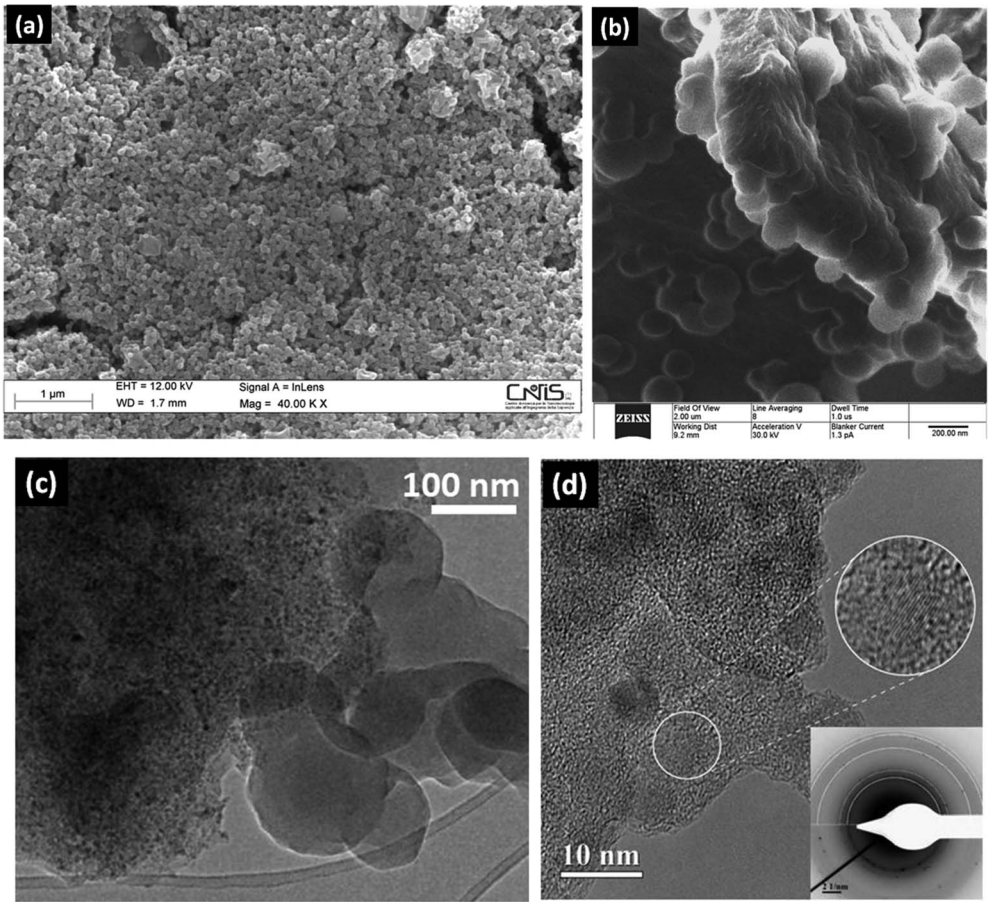

Fig. 7 Pictures relating to the morphological study carried out on the PEDOT–ND sample EAD: (a) SEM image; (b) HIM image; (c) TEM image; and (d) high resolution TEM image with the related ED pattern.

3.3.2 Topography and 3D spatial order. The morphological and 3D structural information of all the samples has been gathered through the combination of several diagnostic techniques, such as scanning and transmission electron microscopy (SEM, TEM), helium ion microscopy (HIM), electron diffraction (ED), and X-ray diffraction (XRD). In particular, HIM is a novel microscopic technique distinguished by the absence of the charging or blurring effects traditionally associated with SEM and therefore well suited to imaging those samples, like polymeric materials, extremely sensitive to electron beam sources. Some selected images obtained by these advanced techniques are displayed in Fig. 5 and 7–9.

Comparing the general morphology of the pure PEDOT systems (EA, $EA_{1/2}$, $EA_{1/4}$) (Fig. 5), we can observe that the polymer grows producing spherical nanostructures whose surface roughness and organization at micro-scale seem to be influenced by the APS amount used in the reaction. According to the mechanism proposed above, the spherical shape is presumably induced by the soft-template constituted by the EDOT droplets stabilized by the dodecyl sulfate micelles formed in the aqueous reaction environment. Such occurrence has been pointed out also in other studies.[4,42] Anyway, unlike what was found by Z. Guo *et al.*[43] on the effect of the molar ratio between EDOT and the oxidant $FeCl_3$ on the PEDOT morphology, in the present study the sphere-shaped structure remains the prevalent morphology for PEDOT, independently of the molar ratio between the monomer and APS oxidant. Obviously, the different experimental conditions (surfactant, oxidant, temperature, *etc.*) under which the two experiments were conducted can easily explain such divergent results.

The high-magnification TEM images help to highlight the morphology of the spheres with a greater detail. The inset in Fig. 5b reveals that the EA sample is constituted by aggregates of quasi-spherical particles with an average diameter of 165 nm and widespread surface asperities (marked by two white circles). Moreover, the transmitted electronic beam clearly evidences that such particles are actually formed by a stacking of polymer layers. A considerable reduction of size and surface roughness of the PEDOT spheres is found for the samples $EA_{1/2}$ and $EA_{1/4}$ (Fig. 5c and e), for which average diameters of about 60 and 20 nm can be respectively assigned. For these samples, no particular structural organization is evidenced inside the spheres (insets of Fig. 5d and f) which result to be particularly sensitive to the electron beam exposure during prolonged TEM investigation (inset of Fig. 5f).

A confirmation of the different spatial order of the polymer chains comes from XRD experimental spectra (Fig. 6). In particular, in the EA spectrum (Fig. 6a) we can observe two

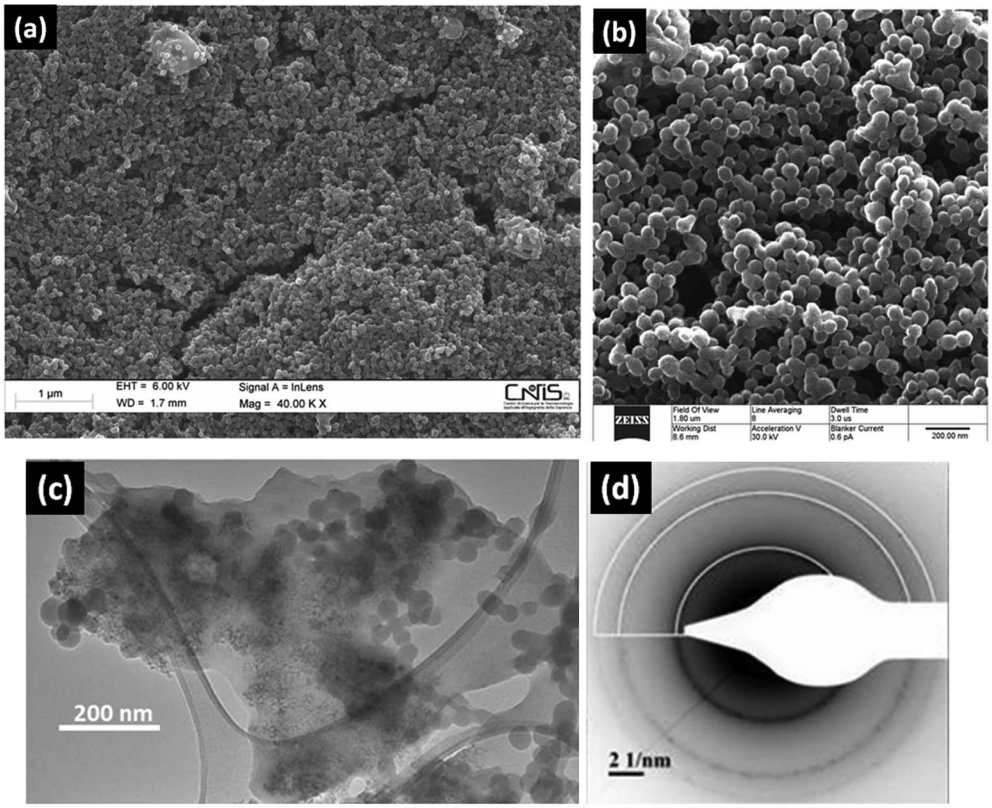

Fig. 8 Pictures relating to the morphological study carried out on the PEDOT–ND sample $EA_{1/2}D$: (a) SEM image; (b) HIM image; (c) TEM image; and (d) ED pattern.

broad peaks at 2θ scattering angles of 12.5° and 25.0° whereas only a broad peak at 25.0° is seen in both the spectra of $EA_{1/2}$ and $EA_{1/4}$ (Fig. 6b and c). As discussed in the literature by several authors, it appears reasonably that PEDOT chains, like in the case of the widely studied poly(3-alkyl thiophene)s, pack in an orthorhombic lattice with a piled lamellar structure of conjugated sheets stabilized by inter-chains π–π stacking.[44–47] In this frame, we can assign the peak at $2\theta \approx 12.5°$ to the (200) reflection, with a calculated *d*-spacing of about 3.6 Å,[46] and the peak centered at 25° to the (020) reflection. These two peaks can be ascribable to the periodicity parallel and normal (π–π inter-chains stacking) to PEDOT backbones, respectively.[47–49] For the sake of clarity, molecular sketches illustrating the PEDOT chains orientation along the 200 and 020 crystallographic directions collected by XRD are reported along with each spectrum in Fig. 6. In the $EA_{1/2}$ and $EA_{1/4}$ spectra, the registered large peak centered at 25° actually shows a shoulder that can be reasonably referred to the peak at 12.5°. This result could be explained by an arrangement of the PEDOT chains characterized by a reduced structural order, which persists mainly along the direction of inter-layers stacking (020). According to the findings of the optical analysis, such results point out that the increase of the EDOT:APS molar ratio (*i.e.* decreasing the amount of APS) induces a worsening of the polymerization process leading to shorter and poorly packed polymer chains.

A different scenario can be described when the morphology and the structure of the PEDOT–ND composites (EAD, EA1/2D, EA1/4D) are analyzed (Fig. 7–10). Although the nanospheres appear in every sample, the effects of different concentrations of APS seem to be less obvious. The comparison between EA and EAD (Fig. 5b and 7b) shows a lower surface roughness of the particles constituting the latter sample and a visible smooth surface effectively characterizes the nanospheres of $EA_{1/2}D$ and $EA_{1/4}D$ (Fig. 8b and 9b). Nevertheless, the size of the particles still seems to be influenced by the concentration of the oxidant, exhibiting values similar to those of the samples without nanodiamonds. But what distinguishes the composite with respect to the pure polymer samples is the assembling of the PEDOT particles at the micro-scale to produce compact films for every concentration of APS (Fig. 5a, c and e, 7a, 8a, and 9a). In general, it can be seen as these layers are constituted by a combination of spheres and platelets (see as an example Fig. 7b). The location of ND within these structures is evidenced by ED patterns and confirmed by TEM images. Fig. 7c and d, 8c and d and 9c and d reveal that ND represents the core of the platelets and show the typical diffraction rings of diamond due to the cubic symmetry of the space group *Fd3m* with unit cell dimensions of $a = b = c = 0.357$ nm as calculated on the basis of the standard values (JCPDS card #06-0675). High resolution TEM images absolutely confirm the presence of diamond embedded into the polymeric matrix and evidence its capability to improve the polymer stability under the radiation effects of the electron beam. In particular, in Fig. 6d diamond fringes surrounded by the polymer are clearly seen, and the related ED

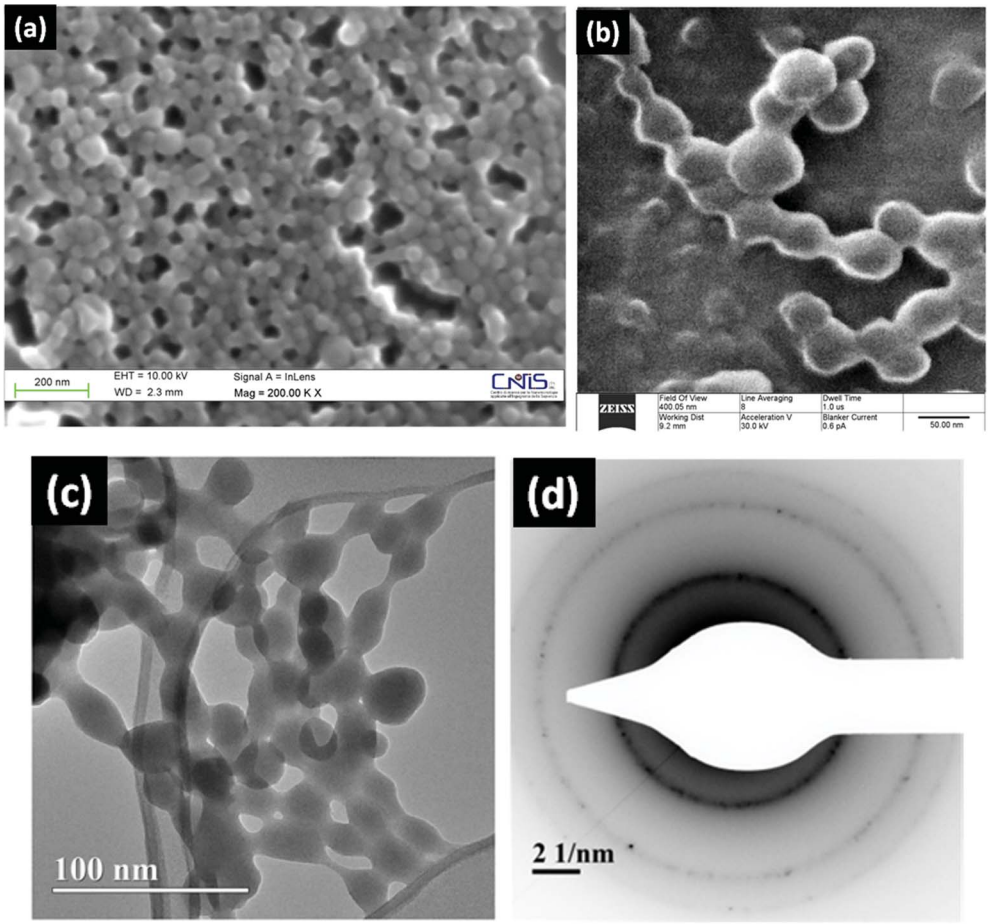

Fig. 9 Pictures relating to the morphological study carried out on the PEDOT–ND sample $EA_{1/4}D$: (a) SEM image; (b) HIM image; (c) TEM image; and (d) ED pattern.

pattern indicates an interplanar distance of 0.206 nm corresponding to (111) plane reflection.

The occurrence of structural interaction between PEDOT and ND is also supported by XRD analysis. In the diffraction experimental spectra of all the composite materials (EAD, $EA_{1/2}D$, $EA_{1/4}D$) (Fig. 10a–c), the three main reflections (111), (220), and (331) corresponding to the nanodiamond cubic phase and the peaks associable to the (200) and (020) reflections of the orthorhombic crystal arrangement of PEDOT are easily recognizable. Furthermore, in the EAD spectrum (Fig. 10a) a peak at scattering angle $2\theta \approx 6^\circ$ is visibly manifested that can be attributed to the (100) reflection of the PEDOT backbones.[46] A reduction of the peak width for the signals of all the composites compared to the analogous ones of the pure polymer samples is also detected. Since such parameter is related to the crystalline correlation length or to the degree of distortions from the perfect crystalline lattice, its reduction in the composite materials implies that PEDOT–ND possess a better structural order than the bare PEDOT samples. In addition, an interesting trend is found for both pure and composite materials. A shift of the peak line regarding the (020) reflection towards higher angles with increasing the concentration of the APS in the polymerization process is observed and results particularly marked in the EAD spectrum (Fig. 10a). The occurrence of such shift corresponds to a decrease in the stacking distance of PEDOT chains[17] and is associated with the increase of the doping level of the polymer.[48]

In conclusion, we can deduce that although the similarity of the XRD spectra of the pure and composite samples suggests an analogous arrangement of the PEDOT chains for the two typologies of materials, a superior spatial organization is induced when ND is used as a filler. Such an effect appears to be particularly evident when the same molar concentration is used for the main reagents like it happens for the EAD sample. In this view, ND can be considered an active filler able to react during the EDOT polymerization since not only it showed the ability to catalyze the start of the reaction, but also to generate longer and more packed PEDOT chains as a reliable structure-directing agent. The aptitude of ND to take part in the polymerization reaction as well as to induce a greater structural order can be due to the several properties that this material possesses. As previously suggested, the presence of functional groups, even radical, on the surface of the ND particles may explain a synergistic action for the EDOT polymerization reaction. Moreover, both the facet-dependent variations of the surface electrostatic potential and the hydrophilicity of the polyhedral

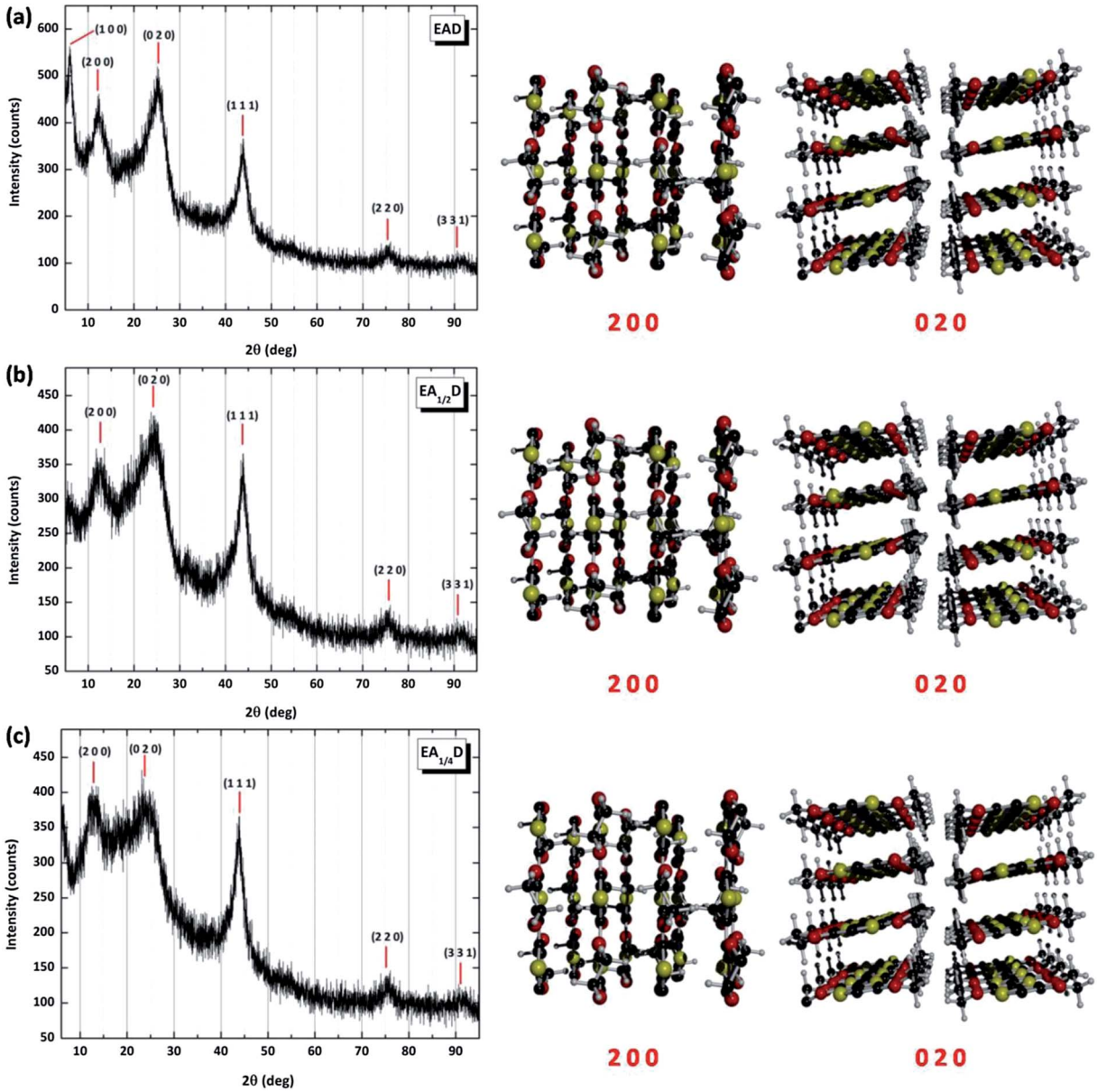

Fig. 10 XRD spectra and depictions of parallel (200) and normal (020) periodicity of the polymer backbones of PEDOT–ND composite samples: (a) EAD; (b) $EA_{1/2}D$; and (c) $EA_{1/4}D$.

ND particles[3,30,50] can provide multi-interfaces where the PEDOT nucleation process can take place and moreover suitable for modulating the orientation of the polymer backbones.

4. Functional properties

Conductive PEDOT films obtained by coating or printing the polymer aqueous dispersion are widely used for the fabrication of antistatic materials for the packaging of electronic components and as protection films for flat panel displays. In particular, in order to allow easy charge migration but to avoid high currents, antistatic agents with low content of large particles, sufficient hardness, high adhesion properties, and a surface resistance ranging between 10^5 and 10^{11} Ω sq^{-1} are typically required.[34]

In view of a possible application in this field, electrical and mechanical functional tests have been carried out on the new materials produced in the present research. In particular, coatings of poly(ethylenterephthalate) (PET) substrates by using EA and EAD were achieved by dip-casting the EA and EAD aqueous dispersions producing the PEDOT/PET and PEDOT–ND/PET systems (Fig. 11a). Thicknesses of about 10 μm have been estimated by profilometer measurements for both the systems.

In Fig. 11b a typical *I–V* curve obtained from PEDOT–ND/PET systems by a four probe method is shown. An ohmic response is detected in the range of the investigated potentials, and a

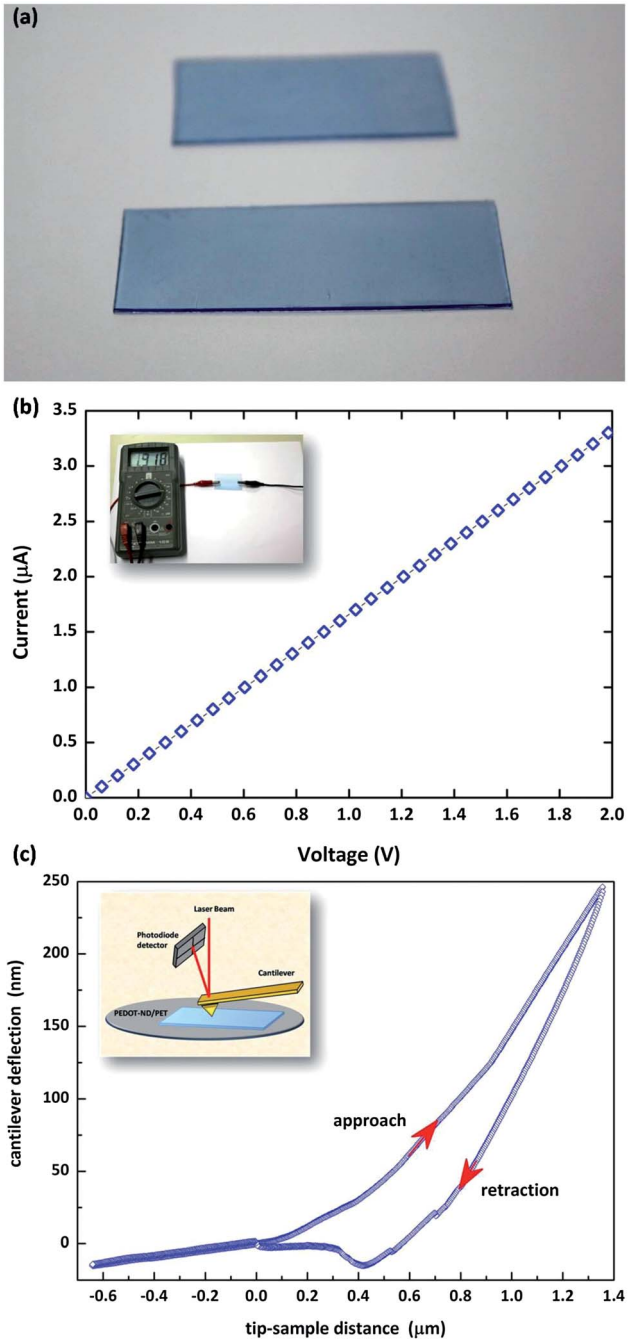

Fig. 11 (a) Poly(ethylenterephthalate) substrates totally coated by the EAD sample (PEDOT–ND/PET); (b) a *I*–*V* curve obtained from the PEDOT–ND/PET system by a four probe method with an inset showing the electrical conductivity of the system; (c) AFM indentation curve obtained on the PEDOT–ND/PET system and a sketch of the measurements setup.

surface resistance value of about $1 \times 10^6\ \Omega\ \mathrm{sq}^{-1}$ is calculated by using the equation:

$$\rho_S = \frac{V}{I}\frac{d}{s}C' \quad (1)$$

where d, s, and C' are parameters depending on the geometry of the samples and on the measurement setup.[51] As regards the pure PEDOT, analysis of PEDOT/PET systems gave sheet resistance values of about $8 \times 10^7\ \Omega\ \mathrm{sq}^{-1}$. The better performance shown by the nanocomposite is likely a consequence of the good stacking of the PEDOT conjugated segments due to the formation, induced by ND, of a higher number of ordered regions where the inter-chains overlap among the π orbitals is more effective, and a valuable charge transport is consequently produced. According to this picture, it is reasonably explained why the presence of an electrically insulating inclusion, such as ND, does not affect but rather contributes to enhance the conductive properties of the PEDOT host. Such an effect can be considered a further confirmation of the existence of a concrete synergy between the two constituents of the composite material.

The mechanical investigations were carried out by depth sensing indentation (DSI) by AFM. This technique allows the limitations associated with a standard DSI setup in the measuring polymeric films to be overcome, whose low values of the elastic modulus require the application of loads lower than those usually adopted in standard techniques.[21] The possibility given by AFM indentation of characterizing local mechanical properties at a sub-micrometrical and nanometric scale allows valuable information to be derived for the understanding of intimate interactions among the materials' component blends and alloys. In Fig. 11c the characteristic AFM indentation curve for the PEDOT–ND/PET system is reported. The analysis of the curves obtained for both PEDOT–ND/PET and PEDOT/PET systems in different regions of the samples revealed an overall improvement of the mechanical properties of the nanocomposite with respect to the pure polymer. In particular, a ratio of 2.6 ± 0.3 between the values of indentation modulus and a ratio of 3.1 ± 0.5 between the values of indentation hardness of the composite with respect to the pure polymer have been found. These results confirm that the method of synthesis has led to the production of a homogeneous dispersion of the ND filler inside the PEDOT matrix, and that the final composite material benefits from a valuable combination of the two components' properties.

5. Conclusions

The present research allows some interesting conclusions to be derived concerning the use of detonation nanodiamond particles as a filler for the production of PEDOT based composite nanostructures by a template-free chemical polymerization method.

First of all, it has been evidenced that ND particles are responsible for a high catalytic activity on the monomer polymerization rate and for hierarchical effects on the arrangement of PEDOT backbones. The presence of nanodiamonds in the reaction medium induces the formation of longer PEDOT chains, and contributes to generate highly conjugated and doped systems. At the same time, also the spatial distribution of ND is influenced by the organization of polymer segments.

It was demonstrated as it is possible to produce PEDOT–nanodiamond composites with a high transparence in the visible range and able to form compact films constituted by

smooth surface nanospheres with an exceptional 3D structural order. Such systems are characterized by considerable charge transport properties and by an enhancement of the mechanical properties and of the endurance to electrons damage with respect to the pure polymer. All these functionalities make these innovative materials highly interesting as candidates for transparent polymeric electrodes and antistatic coatings for the packaging of electronic components.

In conclusion, the capability of producing PEDOT nanostructures with controlled structural order and functional properties by a proper choice of the polymerization method and of the use of an outstanding filler like ND opens the way for a low cost and low environmental impact mass production of efficient multifunctional nanocomposites that can find applications in the most varied and advanced technological fields.

Acknowledgements

The authors are grateful for the support of the European Research Infrastructure EUMINAfab (funded under the FP7 specific program Capacities, Grant Agreement Number 226460) and the Advanced Microscopy Laboratory (AML) in CRANN for the provision of their facility and expertise. The authors are also pleased to thank Dr Dariush Hampai and Dr Carlotta Marianecci for their technical support and advice concerning, respectively, the structural characterization by X-ray diffraction, performed at XLab of "Laboratori Nazionali di Frascati", and the DLS and ζ-potential measurements. ET wishes to thank Mr Marco Rovina for his unconditional support.

References

1 T. L. Kelly, K. Yano and M. O. Wolf, *ACS Appl. Mater. Interfaces*, 2009, **1**(11), 2536–2543.
2 Y. Z. Long, M. M. Li, C. Gu, M. Wan, J. L. Duvail, Z. Liu and Z. Fan, *Prog. Polym. Sci.*, 2011, **36**, 1415–1442.
3 H. J. Ding, C. J. Zhu, Z. M. Zhou, M. X. Wan and Y. Wei, *Macromol. Rapid Commun.*, 2006, **27**, 1029–1034.
4 M. X. Wan, *Adv. Mater.*, 2008, **20**, 2926–2932.
5 M. L. Terranova, V. Guglielmotti, S. Orlanducci, V. Sessa, D. Sordi, E. Tamburri, F. Toschi, L. Palumbo, A. Valloni and M. Rossi, *Crystallogr. Rep.*, 2010, **55**(7), 1223–1226.
6 E. Tamburri, S. Orlanducci, V. Guglielmotti, G. Reina, M. Rossi and M. L. Terranova, *Polymer*, 2011, **52**, 5001–5008.
7 E. Tamburri, V. Guglielmotti, S. Orlanducci, M. L. Terranova, D. Sordi, D. Passeri, R. Matassa and M. Rossi, *Polymer*, 2012, **53**, 4045–4053.
8 V. N. Mochalin, O. Shenderova, D. Ho and Y. Gogotsi, *Nat. Nanotechnol.*, 2012, **7**(1), 11–23.
9 J. Y. Raty and G. Galli, *Nat. Mater.*, 2003, **2**(12), 792.
10 E. Tamburri, S. Orlanducci, F. Toschi, M. L. Terranova and D. Passeri, *Synth. Met.*, 2009, **159**, 406–414.
11 E. Tamburri, V. Guglielmotti, S. Orlanducci and M. L. Terranova, *Inorg. Chim. Acta*, 2011, **377**, 170–176.
12 E. Tamburri, S. Sarti, S. Orlanducci, M. L. Terranova and M. Rossi, *Mater. Chem. Phys.*, 2011, **125**, 397–404.
13 J. Liu and M. Wan, *J. Mater. Chem.*, 2001, **11**, 404–407.
14 J. Jang, M. Chang and H. Yoon, *Adv. Mater.*, 2005, **17**, 1616–1620.
15 J. Jang, J. Bae and E. Park, *Adv. Mater.*, 2006, **18**, 354–358.
16 M. G. Han and S. H. Foulger, *Small*, 2006, **2**(10), 1164–1169.
17 C. A. Dai, C. J. Chang, H. Y. Chi, H. T. Chien, W. F. Su and W. Y. Chiu, *J. Polym. Sci., Part A: Polym. Chem.*, 2008, **46**, 2536–2548.
18 D. Yin, Y. Li, Z. Huang, H. Gu and Z. Wang, *Polymer*, 2011, **52**, 4785–4791.
19 Z. Guo, Y. Qiao, H. Liu, C. Ding, Y. Zhu, M. Wan and L. Jiang, *J. Mater. Chem.*, 2012, **22**(33), 17153–17158.
20 A. Ispas, R. Peipmann, B. Adolphi, I. Efimov and A. Bund, *Electrochim. Acta*, 2011, **56**, 3500–3506.
21 D. Passeri, A. Bettucci, A. Biagioni, M. Rossi, A. Alippi, E. Tamburri, M. Lucci, I. Davoli and S. Berezina, *Ultramicroscopy*, 2009, **109**, 1417–1427.
22 A. M. Schrand, S. A. Ciftan Hens and O. A. Shenderova, *Crit. Rev. Solid State Mater. Sci.*, 2009, **34**(1), 18–74.
23 *Conducting Polymers, Fundamentals and Applications*, ed. P. Chandrasekhar, Kluwer Academic Publishers, Boston, MA, 1999.
24 F. Minisci, A. Citterio and C. Giordano, *Acc. Chem. Res.*, 1983, **16**(1), 27–32.
25 D. Su, N. I. Maksimova, G. Mestl, V. L. Kuznetsov, V. Keller, R. Schlögl and N. Keller, *Carbon*, 2007, **45**, 2145.
26 J. Zhang, D. Sheng Su, R. Blume, R. Schlögl, R. Wang, X. Yang and A. Gajovic, *Angew. Chem., Int. Ed.*, 2010, **49**, 8640–8644.
27 D. S. Su, J. Zhang, B. Frank, A. Thomas, X. Wang, J. Paraknowitsch and R. Schlögl, *ChemSusChem*, 2010, **3**, 169.
28 E. A. Tveritinova, I. I. Kulakova, Y. N. Zhitnev, A. V. Fionov, A. Lund, W. Chen, I. Buyanova and V. V. Lunin, *Russ. J. Phys. Chem.*, 2012, **86**, 26–31.
29 J. M. Carlsson and M. Scheffler, *Phys. Rev. Lett.*, 2006, **96**, 046806.
30 L. Y. Chang, E. Osawa and A. S. Barnard, *Nanoscale*, 2011, **3**, 958–62.
31 A. M. Panich, A. I. Shames, B. Zousman and O. Levinson, *Diamond Relat. Mater.*, 2012, **23**, 150–153.
32 S. B. Orlinskii, R. S. Bogomolov, A. M. Kiyamova, B. V. Yavkin, G. M. Mamin, S. Turner, G. Van Tendeloo, A. A. Shiryaev, I. I. Vlasov and O. Shenderova, *Nanosci. Nanotechnol. Lett.*, 2011, **3**(1), 63–67.
33 A. I. Shames, V. Y. Osipov, A. E. Aleksenskiy, E. Ōsawa and A. Ya. Vul', *Diamond Relat. Mater.*, 2011, **20**, 318–321.
34 A. Elschner, S. Kirchmeyer, W. Lovenich, U. Merker and K. Reuter, *PEDOT: Principles and Applications of an Intrinsically Conductive Polymer*, CRC Press Taylor & Francis Group, 2011.
35 T. A. Skotheim, R. L. Elsenbaumer and J. R. Reynolds, *Handbook of Conducting Polymers*, M. Dekker, New York, 2nd edn, 1998.
36 S. Garreau, G. Louarn, J. P. Buisson, G. Froyer and S. Lefrant, *Macromolecules*, 1999, **32**, 6807–6812.
37 J. Ouyang, Q. F. Xu, C. W. Chu, Y. Yang, G. Li and J. Shinar, *Polymer*, 2004, **45**, 8443–8450.

38 J. Ouyang, C. W. Chu, F. C. Chen, Q. F. Xu and Y. Yang, *J. Macromol. Sci., Part A: Pure Appl.Chem.*, 2004, **41**, 1497–1511.
39 V. N. Mochalin, O. Shenderova, D. Ho and Y. Gogotsi, *Nat. Nanotechnol.*, 2012, **7**, 11–23.
40 M. Akimoto, Y. Furukawa, H. Takeuchi, I. Harada, Y. Soma and M. Soma, *Synth. Met.*, 1986, **15**, 353.
41 R. Malavé Osuna, V. Hernández, J. T. López Navarrete, J. Aragó, P. M. Viruela, E. Ortí, Y. Suzuki, S. Yamaguchi, J. T. Henssler and A. J. Matzger, *ChemPhysChem*, 2009, **10**, 3069–3076.
42 Z. X. Wei, Z. Zhang and M. X. Wan, *Langmuir*, 2002, **18**, 917.
43 Z. Guo, Y. Qiao, H. Liu, C. Ding, Y. Zhu, M. Wan and L. Jiang, *J. Mater. Chem.*, 2012, **22**, 17153.
44 T. J. Prosa, M. J. Winokur, J. Moulton, P. Smith and A. J. Heeger, *Macromolecules*, 1992, **25**, 4364–4372.
45 H. Sirringhaus, P. J. Brown, R. H. Friend, M. M. Nielsen, K. Bechgaard, B. M. W. Langeveld-Voss, A. J. H. Spiering, R. A. J. Janssen, E. W. Meijer, P. Herwig and D. M. de Leeuw, *Nature*, 1999, **401**, 685–688.
46 K. E. Aasmundtveit, E. J. Samuelsen, L. A. A. Pettersson, O. Inganas, T. Johansson and R. Feidenhans, *Synth. Met.*, 1999, **101**, 561–564.
47 E. G. Kim and J. L. Brédas, *J. Am. Chem. Soc.*, 2008, **130**, 16880–16889.
48 J. W. Choi, M. G. Han, S. Y. Kim, S. G. Oh and S. S. Im, *Synth. Met.*, 2004, **141**, 293–299.
49 Y. Li, Y. Feng and W. Feng, *Synth. Met.*, 2012, **162**, 781–787.
50 J. Stejskal, I. Sapurina and M. Trchová, *Prog. Polym. Sci.*, 2010, **35**, 1420–1481.
51 F. M. Smits, *Bell Syst. Tech. J.*, 1958, **37**, 711.